Biosensors and Bioelectronics

A Portable Elliptical Dichroism Spectrometer Targeting Secondary Structural Features of Tumorous Protein for Pancreatic Cancer Detection

--Manuscript Draft--

Manuscript Number:	BIOSBE-D-22-03622R1
Article Type:	Full Length Article
Section/Category:	The others
Keywords:	Elliptical Dichroism; Circular dichroism; Spectrometer; Stereochemical Analysis, Chiroptical, Cancer Detection, Density-Functional Theory
Corresponding Author:	Dali Sun, Ph.D. North Dakota State University Fargo, North Dakota UNITED STATES
First Author:	Aaron Bauer, M.S.
Order of Authors:	Aaron Bauer, M.S.
	Santhalingam Elamurugan, M.S.
	Sara Tolba Selim
	Fatima Fatima, Ph.D
	Ejjigu Nega, M.S.
	Ivan T. Lima, Ph.D
	Wenjie Xia, Ph.D
	Dali Sun, Ph.D.

A Portable Elliptical Dichroism Spectrometer Targeting Secondary Structural Features of Tumorous Protein for Pancreatic Cancer Detection

Aaron Bauer,[1] Santhalingam Elamurugan,[1] Sara Tolba Selim,[2] Fatima,[3,4] Ejjigu Nega,[1] Ivan T. Lima Jr.,[5] Wenjie Xia,[1,2,4] Dali Sun[1,5]*

[1] Biomedical Engineering Program, North Dakota State University, 1401 Centennial Blvd, Engineering Administration, Room 203, Fargo, ND 58102.

[2] Materials and Nanotechnology Program, North Dakota State University, 1410 North 14th Avenue, CIE 201, Fargo, ND 58102.

[3] Department of Mathematics, Computer Science and Physics, Roanoke College, Salem, VA 24153.

[4] Department of Civil, Construction and Environmental Engineering, North Dakota State University, 1410 North 14th Avenue, CIE 201, Fargo, ND 58102.

[5] Department of Electrical and Computer Engineering, North Dakota State University, 1411 Centennial Blvd., 101S Fargo, ND 58102.

Corresponding author: Tel.:+ 1 701-231-6659; E-mail address: dali.sun@ndsu.edu

Keywords: *Elliptical Dichroism, Circular Dichroism, Spectrometer, Stereochemical Analysis, Chiroptical, Cancer Detection, Density-Functional Theory*

Abstract

Stereochemical analysis is essential for understanding the complex function of biomolecules. Various direct and indirect approaches can be used to explore the allosteric configuration. However, the size, cost, and delicate nature of these systems limit their biomedical usage. Here, we constructed elliptical dichroism (ED) spectrometer for biomedical applications, whose performance is validated by experiment and theoretical simulation (Jones/Mueller calculus and time-dependent density-functional theory). Instead of complicated control of circular polarization, ED spectrometer adopted the absorbance of left- and right-oriented elliptically polarized light. With a simplified design, we demonstrated the potential of ED spectrometry as an alternative for secondary structural analysis of biomolecules, their conformation and chirality. It not only provides a portable, low-cost alternative to the sophisticated instruments currently used for structural analysis of biomolecules but also provides superior translational features: low sample consumption(200μl), easy operation, and multiple working modes, for noninvasive cancer detection.

1. Introduction

Stereochemical properties play a prominent role in determining the functional parameters of biomolecules and are widely used to evaluate the pharmacodynamic and pharmacokinetic properties of drugs, protein interactions, and biorecognition mechanisms (Bertucci et al., 2010). Various direct and indirect approaches, such as X-ray diffraction (XRD), circular dichroism (CD), or nuclear magnetic resonance (NMR), are commonly used to explore the allosteric configuration of a compound (Bö et al., 2019). However, high-end stereochemical instrumentation is typically benchtop-based with bulky and expensive optical components, moving parts, and a long optical path (Yang et al., 2021a). In particular, the delicate nature of these systems limits their practical use in field hospitals and clinical labs. Even in biomedical research labs, for low-resolution stereochemical analysis, a handy, low-cost, easy-to-use alternative would be substantially beneficial.

Several conventional methods are available to characterize the structure of biomolecules, including XRD, CD, NMR, Fourier-transform infrared (FTIR), Raman spectroscopy, and electron microscopy (Bö et al., 2019; Kaptein et al., 1988; Šali, 1998). Among these technologies, optical rotation is a comparatively easy-to-measure parameter. CD spectroscopy measures the difference in the absorption of left- and right-handed circularly polarized light by the ensemble of peptide bond chromophores in a protein, and thus, is often used to characterize and quantify the content of secondary structures, such as α-helical, β-sheet, and unordered structure of the proteins (Corrêa and Ramos, 2009; Greenfield, 2006; Miles and Wallace, 2019; Venyaminov and Vassilenko, 1994). CD spectroscopy is a nondestructive and fast method providing detailed information for structural analysis. Considering the advantages associated with the technique, most detailed protein analyses involve CD spectroscopy (Kelly and Price, 2005). However, its application is limited by its high cost, bulky assembly, and complexity of the control system in clinical settings, where detailed analysis is unnecessary.

Polarimeter is a cost-effective alternative for stereochemical analysis(Kvittingen and Sjursnes, 2020), which has been well-established for many applications(He et al., 2021). Rotating-wave-plate Stokes Polarimeter (RWPSP) implements a simplified approach of circular polarimetry based on a rotating compensator(Lin et al., 2011). However, polarimetry is underexplored for diagnostics or prognostics due to a lack of accessible stereochemical biomarkers. In our recent study, we found β-sheet rich as a stereochemical feature of pancreatic tumorous cells and

extracellular vesicles (EVs) and their rationale (Rasuleva et al., 2021a), which thus inspires us to utilize polarimetry for cancer detection.

Here, we designed an elliptical dichroism (ED) spectrometer without using an advanced laser source and a polarimeter (Comby et al., 2018; Phan et al., 2021) as a practical solution for low-resolution stereochemical analysis of biomolecules. Unlike conventional CD, ED spectrometers reconstruct elliptical polarization using a combination of linear polarizer and waveplate, avoiding the bulky and expensive optical components, namely, monochromator (MNC), photoelastic modulator (PEM), and photomultiplier tube (PMT); thus, minimizing not only the apparatus size but also the cost of optical rotation measurements. Compared to CD measurement providing detailed insight into the analyte, this ED design with a significantly simplified optical design also reduced the information collected from the measurement. However, validated by theoretical and numerical simulation (Jones/Mueller calculus and time-dependent density-functional theory) and experiments, the ED spectrometry demonstrated adequate performance for chiroptical molecular and protein structural analysis as a low-specification alternative to CD spectrometry for some basic and clinical cancer research. This comprehensive study covers the fundamental theoretical reasoning of ED based on classical optics and quantum mechanical methods, experimental validation of ED on determining structural features of small and macro biomolecules, and the application to the stereochemical analysis of cellular proteins for cancer detection. It provided a convenient, low-cost alternative for daily routine low-specification stereochemical monitoring and demonstrated the potential in distinguishing malignancy by structural features of the tumor-derived proteins, which might contribute to the development of preclinical and clinical noninvasive cancer diagnostics.

2. Experimental section

2.1 Experimental setup

a) Light path and optics design

As demonstrated in Fig. 1, the light path consisted of a deuterium lamp (Hamamatsu, Fig. S1), lever-actuated iris (Thorlabs), UV-fused silica collimator lens with half-inch diameter (Thorlabs), Glan-Taylor prism polarizer (Edmund Optics), quarter waveplate (Karl Lambrecht Corporation), and GaP switchable gain amplified detector (Thorlabs). Optical components were mounted on an aluminum breadboard (8" × 10", Thorlabs).

b) Optomechanical and cage design

We used a compact electrical motorized rotator for the waveplate (Thorlabs). The sample holder was fabricated by 3D printing to accommodate a quartz cuvette (Hellma) with a 1 mm pathlength. Optical and mechanical components were enclosed into an aluminum cage for light shielding and pneumatic sealing. The case was connected to a vacuum system for ventilation of the generated ozone and heat dissipation. The final assembly is illustrated in Fig. 1B.

c) Connection and control

As schemed in Fig. S2, the waveplate motor was connected to a laptop computer through USB cable. The detector was connected to the same laptop through a digital oscilloscope (TBS1000C, Tektronix), which functions as an analog-to-digital converter and debugger. The software was developed to drive the motor and acquire light intensity from the detector simultaneously. All the measurements were acquired five times, and the average was determined for each rotation angle of the waveplate. The intensity data at each rotation angle were stored in the laptop.

2.2 ED measurement

Amino acid and protein samples were prepared in phosphate-buffered saline (PBS, pH 7.4) at 1 mg/ml concentration. 200 µl of the solution was loaded into the sample cuvette covered with lid for the measurements. The system was turned on 30 min prior to each measurement for stable readout (Fig. S3). Before measuring samples, the solvent solution was measured five times and averaged as the blank, which corrected the impact from all optical components (e.g. quartz cuvette) in the lightpath. Each sample was measured five times as well. The absorbance was normalized to the blank using $A(\theta) = log\left(\frac{I_{blank}(\theta)}{I_{sample}(\theta)}\right)$. In the AS mode, the baseline was corrected by a simple linear subtraction connecting the starting and ending points. In the ED mode, ED was calculated as $ED = A_l - A_r$, where A_l and A_r are absorbance at left and right elliptical polarization (θ = 45° and 135°), respectively. Data analysis and graphing were performed using Origin Pro 2020. ED spectrometry (AS mode) measurements of the amino acids are summarized in Fig. S4.

2.3 CD measurements

The CD spectra were recorded using a Jasco J-815 spectropolarimeter (Tokyo, Japan), with a cylindrical cuvette of a 0.1 cm thickness. The light source system was protected by nitrogen (flow rate: 5 L·min^{-1}). Proteins were obtained from cell lysate using a lysis kit (C2978, Sigma-Aldrich) following the manufacturer's protocol. The protein contents in samples were quantified by absorption at 280 nm measured with a Nanodrop ND-1000 spectrophotometer (Thermo Scientific) and diluted to 0.2 mg/ml before CD scan at 200 nm/min in the wavelength region of 200–260 nm. Three scans were averaged for each CD spectrum. Data were analyzed and

processed using the Jasco Spectra Manager 2 software package. CD measurements of the amino acids are summarized in Fig. S5.

2.4 Electronic circular dichroism spectra simulation

All density functional (DFT) calculations were performed by the Gaussian09 program package (M. J. Frisch, G. W. Trucks, H. B. Schlegel et al., n.d.) at 298 K. Initially, molecular structures of amino acids were optimized to their ground state using the Becke's three-parameter hybrid B3LYP (Becke, 1998) exchange-correlation function and the double-zeta polarized 6-31g(d) basis set (Petersson et al., 1998). Using the optimized geometries and at the same theory level, the TD-DFT was employed to calculate excitation energy (eV), excitation wavelength (nm), and rotatory strength R in the dipole velocity (R_{vel}) and dipole length (R_{len}) components (Ding et al., 2007). Next, the ECD spectra, $\Delta\epsilon$ (L mol^{-1} cm^{-1}), were defined as the difference between the left and right molar absorptivity of circularly polarized light and calculated using the following Gaussian function (Stephens and Harada, 2010)

$$\Delta\epsilon\ (E) = \frac{1}{2.297 \times 10^{-39}} \frac{1}{\sqrt{2\pi\sigma}} \sum_{j}^{A} \Delta E_j R_j e^{[-(E-\Delta E_j/2\sigma)]^2}$$

where σ (eV) represents half of the bandwidth at $1/e$ height. E_j (eV) and R_j (10^{-40} cgs) represent the excitation energies and rotatory strengths for transition j, respectively. In this study, σ = 0.33 eV and R_{vel} were used. Optimized amino acid structures for DFT simulation are summarized in Fig. S6. Simulated ECD curves are shown in Fig. S7.

2.5 Simulation of incident light polarization and absorbance

The incident polarization was modeled with the Jones vector, where the polarized light is expressed by a column vector with two rows, and the polarization elements are represented by the 2 × 2 Jones matrix(Goldstein, 2017; Pedrotti et al., 2017). Since a broadband linear polarizer was used, vertical polarized light ($E_i(\lambda) = \sqrt{I_0(\lambda)}\begin{bmatrix}0\\1\end{bmatrix}$) was assumed to be incident on the quarter waveplate (Teare, 2017), where $I_0(\lambda)$ was derived from the light source (Fig. S1).

Jone vector of the waveplate rotated by an angle θ was defined in (Collett, 2005) as

$$J(\psi,\theta) = R(-\theta)J_{QWP}R(\theta)$$

where $R(\theta)$ is a rotation matrix $R(\theta) = \begin{bmatrix}\cos\theta & \sin\theta\\ -\sin\theta & \cos\theta\end{bmatrix}$ and $J_{QWP} = \begin{bmatrix}1 & 0\\ 0 & e^{-i\phi(\lambda)}\end{bmatrix}$

Since the zero-order magnesium fluoride waveplate at 214 nm was used, a linear model was used for simulation: $\phi(\lambda) = 53.5\frac{2\pi}{\lambda}$. The optical field of the beam emerging from the waveplate (E_λ) can be calculated by $E_\lambda = JE_i$.

To model the polarization-dependent absorbance of the sample, we describe the sample by the Mueller matrix $M_{sample} = M_{lb}M_{cb}M_{ld}M_{cd}$ where M_{lb}, M_{cb}, M_{ld}, and M_{cd} are the Mueller matrixes describing the linear birefringence (LB), circular birefringence (CB), and linear dichroism (LD) properties of the sample, respectively(Pham and Lo, 2012). For simulation simplicity, we ignored the matrixes except $\mathrm{M_{cd.}}$ The $\mathrm{M_{cd}}$ was defined as

$$M_{cd}(\lambda) = \begin{pmatrix} \boldsymbol{a}(\lambda) & 0 & 0 & CD(\lambda) \\ 0 & \boldsymbol{a}(\lambda) & 0 & 0 \\ 0 & 0 & \boldsymbol{a}(\lambda) & 0 \\ CD(\lambda) & 0 & 0 & \boldsymbol{a}(\lambda) \end{pmatrix}$$

where $CD(\lambda)$ was derived from CD measurements, and $\boldsymbol{a}(\lambda) = 1 - \frac{A(\lambda)}{A_{max}}$, where $A(\lambda) = \varepsilon(\lambda)cl$ follows Beer-Lambert law (Ball, 2006), c represents the analyte concentration, l represents the light path (0.5 cm), and ε represents molar absorption coefficients measured by a spectrometer (Nanodrop1000, Thermo Scientific, see Fig. S8 for the $\varepsilon(\lambda)$ of BSA).

The output Stokes vector is calculated as $S_{sample} = M_{sample}M_{wpr}S_i$ where $S_i(\lambda)$ was the emergent Stokes vector of the linear polarizer and is given by

$$S_i(\lambda) = I_0(\lambda)\begin{pmatrix} 1 \\ -1 \\ 0 \\ 0 \end{pmatrix}$$

Mueller matrix of the rotating waveplate was constructed as (Goldstein, 2017)

$$M_{wpr}(\phi, \theta) = \begin{pmatrix} \mathbf{1} & 0 & 0 & 0 \\ 0 & \cos^2\theta + \cos\phi \sin^2\theta & (1-\cos\phi)\sin\theta\cos\theta & -\sin\phi\sin\theta \\ 0 & (1-\cos\phi)\sin\theta\cos\theta & \sin^2\theta + \cos\phi\cos^2\theta & \sin\phi\cos\theta \\ 0 & \sin\phi\sin\theta & -\sin\phi\cos\theta & \cos\phi \end{pmatrix}$$

Integrating output Stokes vector over the broadband wavelengths of 200–260 nm restricted by the available CD measurement data, the transmission intensity of the sample $I_{sample}(\theta)$ can be obtained from the first Stokes parameter of the integral $\int S_{sample}(\theta)\, d\lambda = \begin{pmatrix} I_{sample}(\theta) \\ Q(\theta) \\ U(\theta) \\ V(\theta) \end{pmatrix}$.

The absorbance was then calculated as

$$A(\theta) = log\left(\frac{I_{blank}(\theta)}{I_{sample}(\theta)}\right)$$

where $I_{blank}(\theta)$ was calculated using a similar procedure as $I_{sample}(\theta)$ with $S_{blank} = M_{wpr}S_i$. The simulation was conducted using MATLAB with the Mueller–Stokes–Jones Calculus add-in(Vogel, 2022).

2.6 Cell lines and cell culture

The human pancreatic cancer cell lines MIA PaCa-2 and HPNE were obtained from the American Type Culture Collection (Manassas, Virginia). MIA PaCa-2 cells were cultured in DMEM medium (Hyclone, GE Healthcare Life Sciences), and HPNE cells were cultured in DMEM (Hyclone, GE Healthcare Life Sciences) with 0.1ng/ml epidermal growth factor (EGF, Novus Biologicals, USA). All cultures except nonstarvation condition were supplemented with 10% fetal bovine serum (FBS; Life technology, Thermo Scientific Inc.), penicillin (1 U), and streptomycin (1 μg/ml). All cells were maintained in a humidified incubator with 5% CO_2 at 37°C. All cell lines were cultured in triplicate under the same conditions and then harvested to collect independent EV samples. Cell lysates were collected when reached confluence using 100uL Cellytic™ M cell lysis reagent (Sigma-Aldrich) to the culture dish for 30 min. Total protein content in each sample was quantified by a Nanodrop 1000 spectrometer.

2.7 EV isolation from culture media

Cells were grown in culture media with serum until 10^7 cells were obtained, washed three times with phosphate-buffered saline (PBS) (pH 7.0), and then cultured for 48 h in serum-free media(Sun et al., 2021). For nonstarvation condition, the cells were cultured in a medium with 10% EV-depleted FBS (Thermo Scientific, US). Culture supernatants were then filtered by a 0.2 μm filter and centrifuged at 10,000 g for 30 min to remove cell debris. The supernatant was carefully centrifuged at 200,000 g for 70 min. The resulting EV precipitates were collected, dissolved in 100 μL PBS (pH 7.0), and stored at 4°C. TEM (JEOL JEM-2100) and a tunable resistive pulse sensing instrument (qNano system; IZON Science Ltd, Christchurch, New Zealand) were used to validate EV samples.

2.8 Statistics

Comparisons between two groups were performed using an unpaired two-tailed Mann–Whitney U-test (unpaired samples), paired two-tailed Mann–Whitney U-test (paired samples), and two-tailed Student's t-test (normally distributed parameters). Multiple samples were compared using a Sidak multiple comparison test, Kruskal–Wallis test (non-grouped), and ANOVA with Friedman test for multiple comparisons (grouped). All comparison groups had equivalent variances. $p < 0.05$ was considered to be statistically significant. The clustering analysis and the normalized distant map based on ED value were generated using the Hierarchical Cluster Analysis of Origin Pro software. Correlation analysis and other data analyses were performed using Origin Pro software. Matrix correlation was measured by *corrcoef* function from MATLAB. Data were presented either as representative examples or

means ± SEM of 4+ experiments. p values were obtained using unpaired two-tailed Student's t-test or two-way ANOVA. $*p < 0.05$, $**p < 0.01$, and $***p < 0.001$, and $****p<0.0001$.

3. Results

3.1 Concept and design

CD spectroscopy, defined as the unequal absorption of left- and right-handed circularly polarized light, is a sophisticated but excellent rapid indicator of protein secondary structure, folding, and binding properties (Miles and Wallace, 2016). A CD spectrometer utilizes monochromator, polarizer, and PEM to generate right- and left-handed circular polarized light, and a sensitive PMT detector to quantify the analyte absorbance against the oriented circular polarization. Since these major components are bulky, complicated, and expensive, CD spectroscopy consumes several resources.

Inspired by the Rotating-wave-plate Stokes Polarimeter, the combination of linear polarization and rotating waveplate was introduced in our design, as described in Fig. 1A. Although the theoretical model has been established (Goldstein, 2017; Pedrotti et al., 2017; Schellman, 1975), our design tried to avoid an intricated laser source or an expensive polarimeter (Comby et al., 2018; Phan et al., 2021). This combination eliminated PEM. Instead of using MNC for precise wavelength filtering, it was considered that the entire wavelength range of the light as the incident on ED spectrometer might be registered, thus lowering the requirements to the light source intensity and the detector sensitivity, which made it possible to use a low-intensity deuterium lamp and GaP detector, respectively. The deuterium lamp emitted a far UV range (mainly 200-275nm, Fig.S1), covering peptide bond absorption to determine the secondary structure of the proteins (Kelly and Price, 2005). These changes significantly decreased the cost and space of the apparatus, and reduced the complexity of the control system. As demonstrated in Fig. S2, only the waveplate rotation and the synchronization of the detector readout need to be automated in the ED system. A remarkably simplified optical design thus enabled a portable, low-cost spectrometry for stereochemical analysis (Fig. 1B). Fig. 1C describes the advantages of ED compared to CD spectrometers.

To study the theoretical rationale of the ED design, a simulation based on the Jones calculus (see Experimental section for the detailed deduction) was performed to model the polarization generated by the waveplate. Fig. 2 illustrates the simulated polarization ellipse of the ED spectrometer's incident light. We chose a wavelength range covering most of the emission band of the deuterium lamp with corresponding intensity (Fig. S1). Linear polarized light passing through the waveplate forms elliptically polarized light according to the waveplate rotation

angle (θ). As demonstrated in Fig. 2A, the polarization ellipse corresponded to the wavelength of incident linearly polarized light and waveplate rotation angle (θ, Fig. 2A). Each wavelength was characterized by a different tilt of the ellipse at each θ (Movie S1). The waveplate rotation at 45° and 135° represents the polarization ellipses corresponding to right and left elliptical polarization, respectively. Thus, the corresponding absorbance was used to calculate ED. Since none of these two angles generated perfect circular polarization, thus the absorbance difference was named the ED. Following the convention of CD, ED was calculated as $ED = A_l - A_r$, where A_l and A_r represent absorbance at left and right elliptical polarization, respectively (i.e., θ = 45° and 135°).

Selecting the peak wavelength (240 nm) of the light source as an example, the incident light after the rotated waveplate possesses a vertical symmetry in Poincaré sphere (Fig. 2B, left). Poincaré sphere representation (Fig. 2B, right) of the broadband light source reveals the symmetric polarization distribution on the vertical (V) hemisphere across the equatorial plane in respect to the waveplate rotation. The tilt angle and ellipticity angle in the broad range manifested a repeated radical symmetric pattern (Fig. 2C), suggesting the same ellipticity (tilt angle and ellipticity angle) for left and right elliptical polarizations (θ = 45° and 135°) in ED calculation.

3.2 Stereochemical analysis of biomacromolecules using the ED spectrometer

Proteins are linear biomacromolecules of well-defined primary sequences folded for biological functioning (Martz, 2012). The protein structure determines its biological function. The analysis of protein folding (secondary structure) is extensively employed for protein biology studies (Pelton and McLean, 2000). CD is a rapid tool for determining the secondary structure and folding properties of proteins (Greenfield, 2007a). To evaluate ED spectrometry for stereochemical analysis (secondary structure) of a protein, we simulated and measured bovine serum albumin (BSA), a standard reference protein, by ED spectrometry.

As represented in Fig. 1, the spectrometer works in the following two analysis modes: angle sweeping (AS) and ED. In the AS mode, the absorbance (A) was recorded with the waveplate rotation. In ED mode, the absorbance difference is calculated at θ = 45° and 135°. Although the incident polarization varies according to the waveplate angle, the absorbance should be consistent with the Beer-Lambert law (Swinehart, 1962) at each θ for a given analyte in absorption spectrometry:

$$A(\theta) = log\left(\frac{I_{blank}(\theta)}{I_{sample}(\theta)}\right)$$

We thus calculated $I_{blank}(\theta)$ and $I_{sample}(\theta)$ through Mueller calculus, which involves molar absorption of BSA (Fig.S8, see the detailed description in Experimental section). The simulated transmission intensity at each wavelength depends on θ (Fig. 3A), which is consistent with the optical model based on the Jones calculus (Fig. 2A). The broadband absorbance (A) integrated over the wavelength range demonstrated elliptical profiles with reflected elliptical orientation to the transmission intensity (Fig. 3B vers. A), consistent with the Beer-Lambert law.

To demonstrate the potential for secondary structural analysis experimentally, we tested three representative proteins with apparent structural differences using both CD and ED spectrometers. BSA was studied as an α-helix-dominated protein (as labeled in Fig.3D), which was calculated using the bioinformatics method (UniProt) reported in our previous study (Rasuleva et al., 2021a). On the contrary, chymotrypsin and avidin were compared as representatives of β-sheet dominating proteins. CD spectrum of BSA involved an α-helix-rich pattern, while chymotrypsin and avidin contained β-sheet-rich patterns in Fig. 3E (Greenfield, 2007b). Far UV region CD bands corresponding to peptide bond absorption, could be used to analyze secondary structural features. For example, α-helix is featured by negative bands at 222 nm and 208 nm and due to π→π* and n→π* transition, respectively (Miles and Wallace, 2016). However, since ED measurement uses broadband, to be comparable to stepwise monochromatized CD readout, it is only fair to compare areas under the curve (AUC) integrating CD spectra over the wavelength range, with ED. As in Fig. 3F, CD AUCs are apparently different over various structural compositions. AS patterns measured by ED spectrometer were also distinguishable (Fig. 3C). Structural differences were easier discriminated in the ED mode (Fig. 3D), and correlated to the CD AUCs (Fig. 3F). Notably, ED measurements varied more in α-helix-dominating BSA than that in β-sheet-dominating proteins, which may be due to the instability of α-helix folding against UV radiation (Cerpa et al., 1996; Lednev et al., 1999).

3.3 Stereochemical analysis of small biomolecules using the ED spectrometer

Numerous small molecules have molecular asymmetry, where the structure is not superimposable on its mirror image, known as chirality. Among the technologies to measure chirality, optical rotation is comparatively easy to measure. We thus evaluated the potential of using ED for chirality analysis. Conventional CD spectrometry was capable of discriminating L and D forms of amino acids (Fig. 4A and B). Similarly, ED spectrometry yielded distinguishable AS and ED results (Fig. 4C-F). Notably, the AS patterns of L and D forms are

highly analogous (Fig. 4C and D compared to Fig. 3C, analogous vs. non-analogous molecules), implying the potential of this method for analyzing structural proximity.

To evaluate the potential of ED spectrometry for small biomolecule stereochemical analysis, all common soluble amino acids (L form) were experimentally tested by ED and CD spectrometry (Fig. 5A). Theoretically, the molecule configuration can be determined from its optical rotation or electronic circular dichroism (ECD) (Warnke and Furche, 2012). Time-dependent density-functional theory (TD-DFT) was employed to calculate excitation energy and rotatory strength R in the form of dipole velocity (R_{vel}) and dipole length (R_{len}). The calculated rotatory strengths were simulated by an ECD curve (see details in Experimental section), and the AUC was integrated from 200 to 300 nm. ECD represents the theoretical response of molecules to circular polarization from the quantum mechanical point of view. Kendall correlation analysis was performed to study the relation between ED, CD, and ECD. Both ED and CD show a weak correlation with the theoretical ECD (Fig. 5B and C), revealing the inadequacy of using the existing theory (rotation strength) to explain circular/elliptical dichroism of small molecules. However, the ED-ECD correlation was one-order higher compared to that of CD-ECD, suggesting ED as a more effective experimental method for evaluating rotatory strength.

We further verified the ED-based analysis by performing cluster analysis (Fig. 5D). Interestingly, the cluster analysis results coincided with the common amino acid categorization by polarity. Almost all amino acids in group 3 are nonpolar, and those of group 2 are charged. It suggests that ED may be used for the analysis of chemical-physical properties of the molecules. To further explore this possibility, we constructed a distance matrix based on ED (Fig. 5E) and compared the exchangeability matrixes and Epstein's coefficients (Fig. 5F and G), representing the chemical and physical properties, respectively. Experimental exchangeability, the measure of the mean effect of substituting one amino acid with another one (Yampolsky and Stoltzfus, 2005), was depicted as chemical exchangeability. Epstein's coefficient of difference, based on the differences in polarity and size (Epstein, 1967), was selected as a physical and structural reference. The matrix correlation analysis revealed that ED leans two times more to Epstein's coefficient than the exchangeability (0.2910 vs. 0.1672), suggesting that ED may be more suitable for structural analysis responding to physical properties.

3.4 Stereochemical analysis of biological samples using the ED spectrometer for cancer detection

We found the β-sheet richness of the malignant cells and their extracellular vesicles (EVs) in our previous study, and developed a clinical method for cancer screening (Rasuleva et al., 2021a). CD can be used to identify cell lysates and EV from malignant cells (Fig. 6A and B) due to their β-sheet richness, as described in our previous study. The malignant cell is β-sheet rich and exocytoses EVs of the same structural richness, thus corresponding to a lower AUC of CD spectra. To validate the potential clinical application of ED, we tested the potential to discriminate tumorous cells and EVs from nonmalignant counterparts using ED. Malignant cells demonstrated significant differences from nonmalignant counterparts at both cellular and EV levels (Fig. 6C and D). ED follows the trend of CD AUC, indicating the tumor cells and EVs enrichment with β-sheets. These data demonstrate the potential of ED spectrometry for cancer detection.

4. Discussion

In general, there are limited ways of spectrometer miniaturization (Yang et al., 2021b), which necessitates a compromise with respect to degradation of its resolution, dynamic range, or signal-to-noise (SNR) ratio. We reconstructed the method of generating elliptically polarized light, using the combination of a waveplate and a linear polarizer, eliminating the need in PEM modules to generate circularly polarized light. The SNR of CD spectrometer, determined by the PMT and varied with the wavelength, reached 20 (Dinitto and Kenney, 2012). The ED spectrometer possesses a slightly downgraded SNR of approximately 14 (Fig. S9 and Table S2) due to the downgrading of the detector. However, the SNR of ED was optimized by increasing the number of measurements and their average. Therefore, SNRs of CD and ED are comparable. According to the function of the quarter waveplate (Pedrotti et al., 2017) for a linearly polarized incident light, the output polarization should follow the repeating pattern along with θ, as shown in Fig. 2. If a line was drawn from 0° to 180°, the absorbance of the analyte should be radical symmetric against the line. Overall, the broadband absorption was symmetrical in Fig. 3B. However, when the baseline was subtracted, eliminating the impact of the analyte quantity, some of the analytes manifested obvious asymmetry (Fig. 3C, 4C, and D). It can be caused by two possible reasons. The first one might be related to the stability of the analyte under UV light. The waveplate was driven by a step motor, whose angular velocity was restricted by the motor speed and the settling time for acquiring stable output from the detector for each step. Larger θ corresponds to longer UV exposure (Table S1). Therefore, longer UV exposure may

cause stereochemical changes of the analyte, which affect the absorbance. The α-helix to β-sheet transition has been reported under external stimuli (Litvinov et al., 2012; Morillas et al., 2001). UV exposure promoting the α-helix to β-sheet transition (Litvinov et al., 2012) may explain the asymmetry of α-helix-dominated proteins as compared with that of β-sheet-rich proteins (Fig. 3C). Therefore, a possibility to extend ED applications to evaluate the UV analyte stability through asymmetry should be verified. Furthermore, the asymmetry may be caused by the baseline correction method (Blakemore, 1987). We used a linear baseline correction method to compensate for the detector decay along with the light exposure, which was selected considering the simplicity and similar fitting results of the different correction models (similar R^2, Fig. S10). However, this baseline model may not be ideal for all analytes. A unique baseline correction model for each analyte may be necessary to reduce the asymmetry.

CD spectrometry determines a certain wavelength absorbance at high resolution. A CD spectrum of a given protein can be approximated by a linear combination of spectra of the secondary structures, thus evaluating the structural composition of proteins (Greenfield, 2007a). However, most CD-based protein structural analysis methods are empirical (Bulheller and Hirst, 2009; Sreerama and Woody, 2000; Whitmore and Wallace, 2004). Using detailed high-resolution CD spectrometry for the empirical study of protein structure study is not rational. On the contrary, a low-resolution detection by integrating the wavelength range in ED spectrometry is more suitable and handier for the stereochemical analysis of macro biomolecules. Since DNA is more vulnerable to UV light than proteins, we did not test DNA molecules. However, reduced UV emission may potentiate the ED spectrometry for DNA structural analysis.

Liquid biopsy, especially EVs, contains tumor-specific molecules and provides useful real-time information on tumor development (Li et al., 2017). Most of the methods of noninvasive diagnostics based on liquid biopsy have focused on establishing assays that detect the increased expression of a single cancer-associated marker or marker signature based on multiple detections of this biomarker. The disadvantages of these biomarkers are their subtype-specificity, leading to false negatives, or being easily masked by high-background signals, leading to false positives. In addition, the technologies currently used to detect biomarkers in liquid biopsy for cancer screening (immunoassay, LC-MS, qRT-PCR, microarray, and sequencing) are challenging, particularly for low- and middle-income countries, because they require a time-consuming and expensive assay, advanced instrumentation and qualified technicians, large sample volumes (>1ml), and long turnover times, limiting their utility as

clinical screening tests. We previously reported that a malignant cell secretes more β-sheet-rich proteins through EVs as compared to nonmalignant cells. This was the base for the development of a translational method targeting collective attributes of the EVs (Rasuleva et al., 2021b). ED spectrometer with a portable size (8 × 10 × 18 cm) is powerful enough to discriminate malignancy using tumorous EVs, and thus may provide a novel solution for noninvasive cancer diagnostics.

Figures

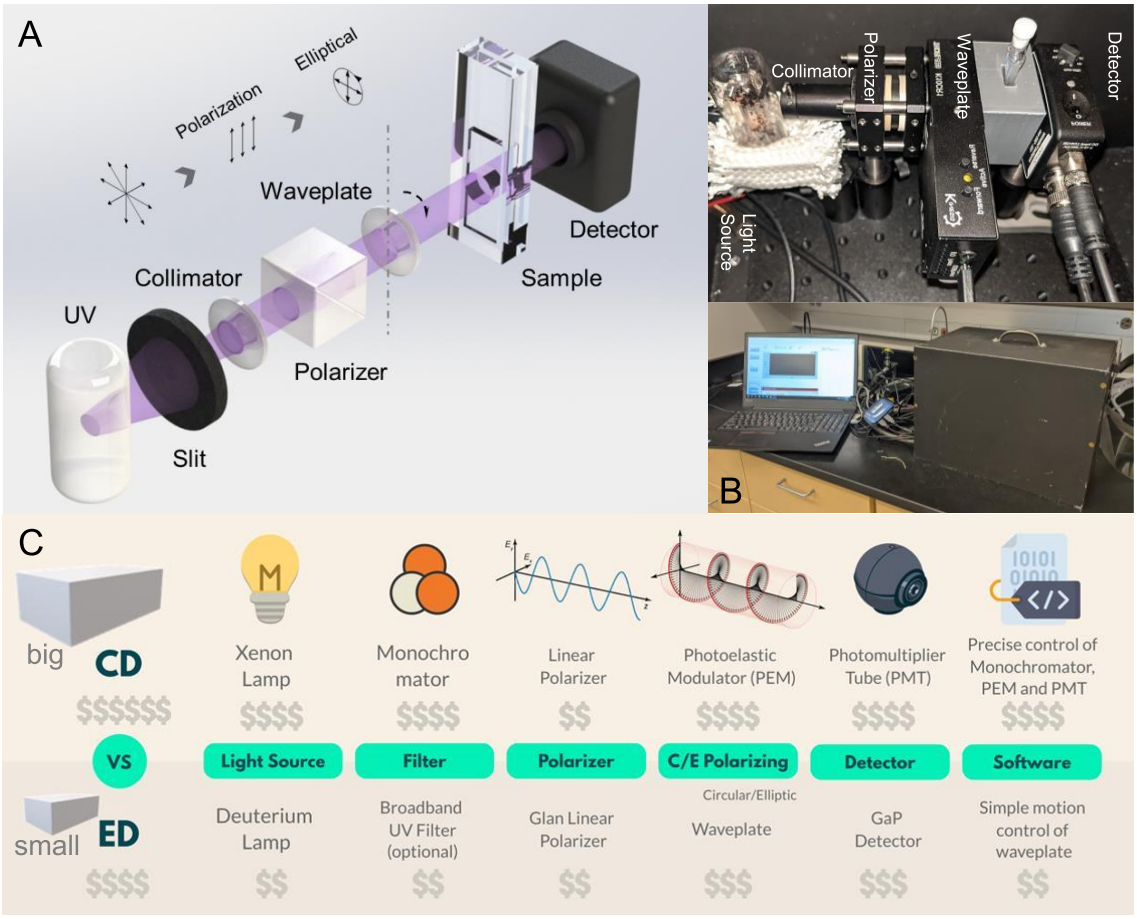

Figure 1. **Elliptical dichroism (ED) spectrometer design.** (**A**). Optical and (**B**) Images of the experimental setup. (**C**) Cost evaluation of circular dichroism (CD) and ED.

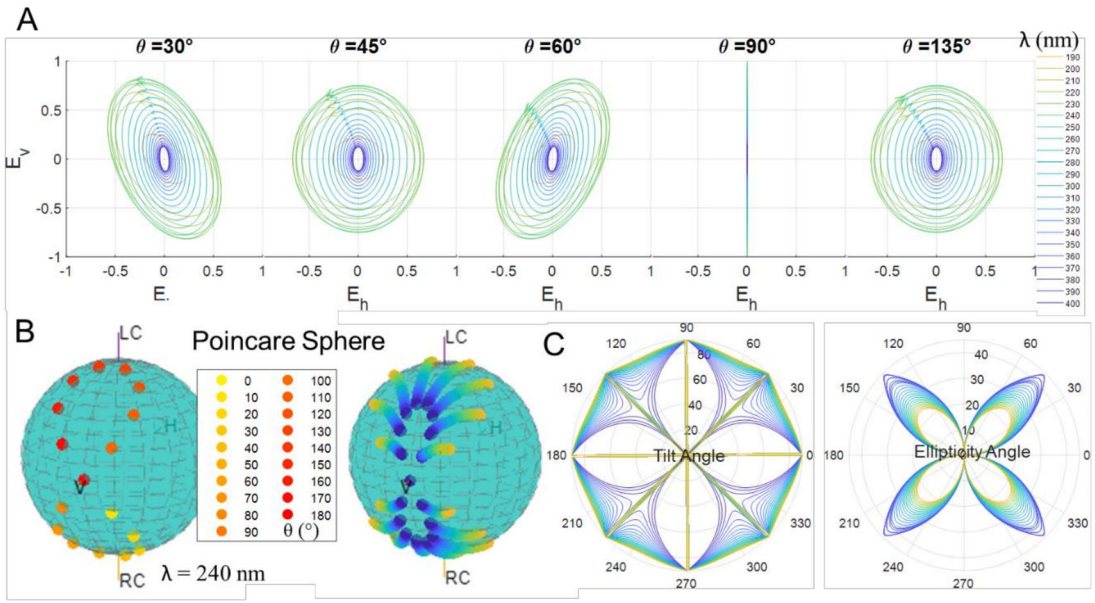

Figure 2. Numerical simulation of the ED by Jones calculus. (A) Polarization ellipse corresponding to wavelength (λ) and waveplate rotation angle (θ). See Movie 1 for polarization ellipses corresponding to the full range of θ**. (B)** Poincaré sphere representation. Single wavelength (left) and multiple wavelengths (right, same legend as **A**). LC/RC: left/right circular symmetry; V/H: vertical/horizontal symmetry. **(C)** tilt angle, ellipticity angle against the wavelength (λ) and waveplate rotation angle (θ), the legend is the same as in **A**.

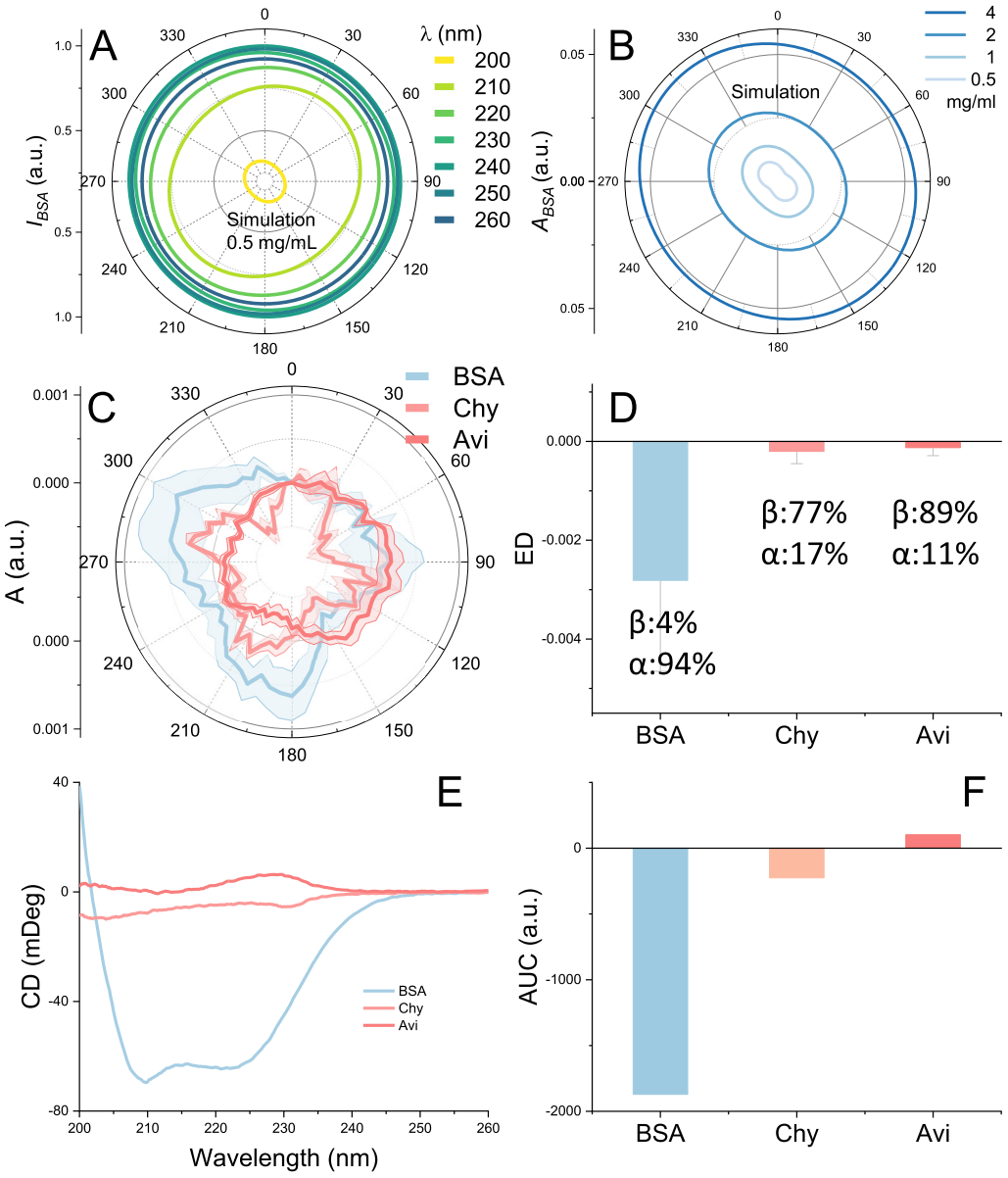

Figure 3. Protein characterization using ED. (**A**) Transmission intensity against the wavelength (λ) and waveplate rotation angle (θ), and (**B**) broadband (200–260 nm) absorption (A) of BSA by Mueller calculus-based simulation. (**C**) and (**D**) Comparison of proteins (0.5 mg/ml) with the different content of the secondary structures using ED under AS and ED modes. The absorbance spectra were baseline subtracted. Secondary structural constitutes were obtained from UniProt. (**E**) CD spectra comparison of proteins (0.5 mg/ml) with the different content of the secondary structures and the area under curve (AUC, **F**). The spectra were averaged on the five repeated measurements. BSA: bovine serum albumin; Chy: chymotrypsin; Avi: avidin. Error bars, mean ± s.e.m; n = 4.

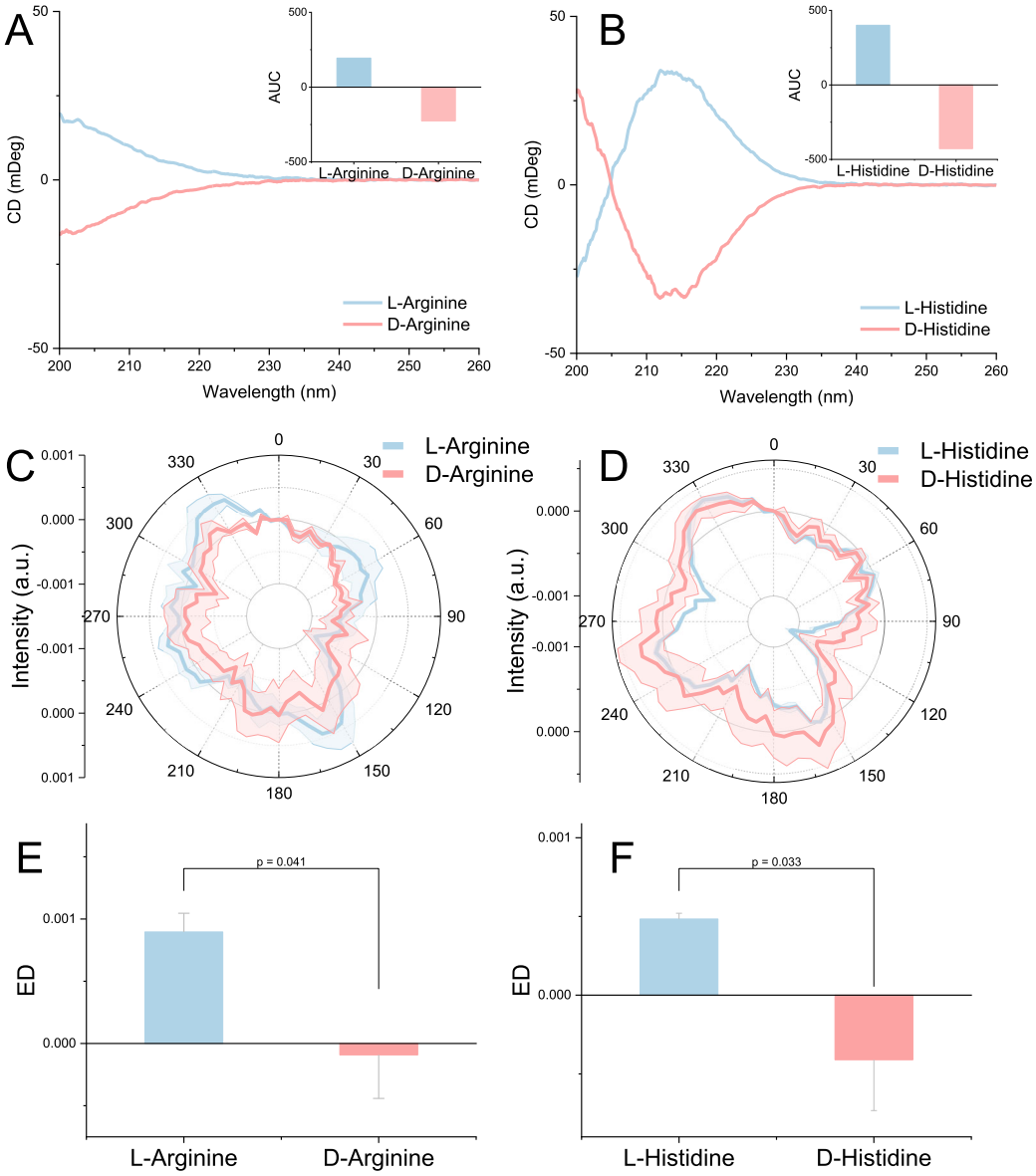

Figure 4. Chirality analysis by ED spectrometry. (**A**) and (**B**) CD spectra and AUCs, (**C**) and (**D**) AS diagrams, (**E**) and (**F**) ED of L and D forms of arginine and histidine, respectively. The CD spectra were averaged from five repeated measurements. The AS diagrams were baseline subtracted. Error bars, mean ± s.e.m; n = 4.

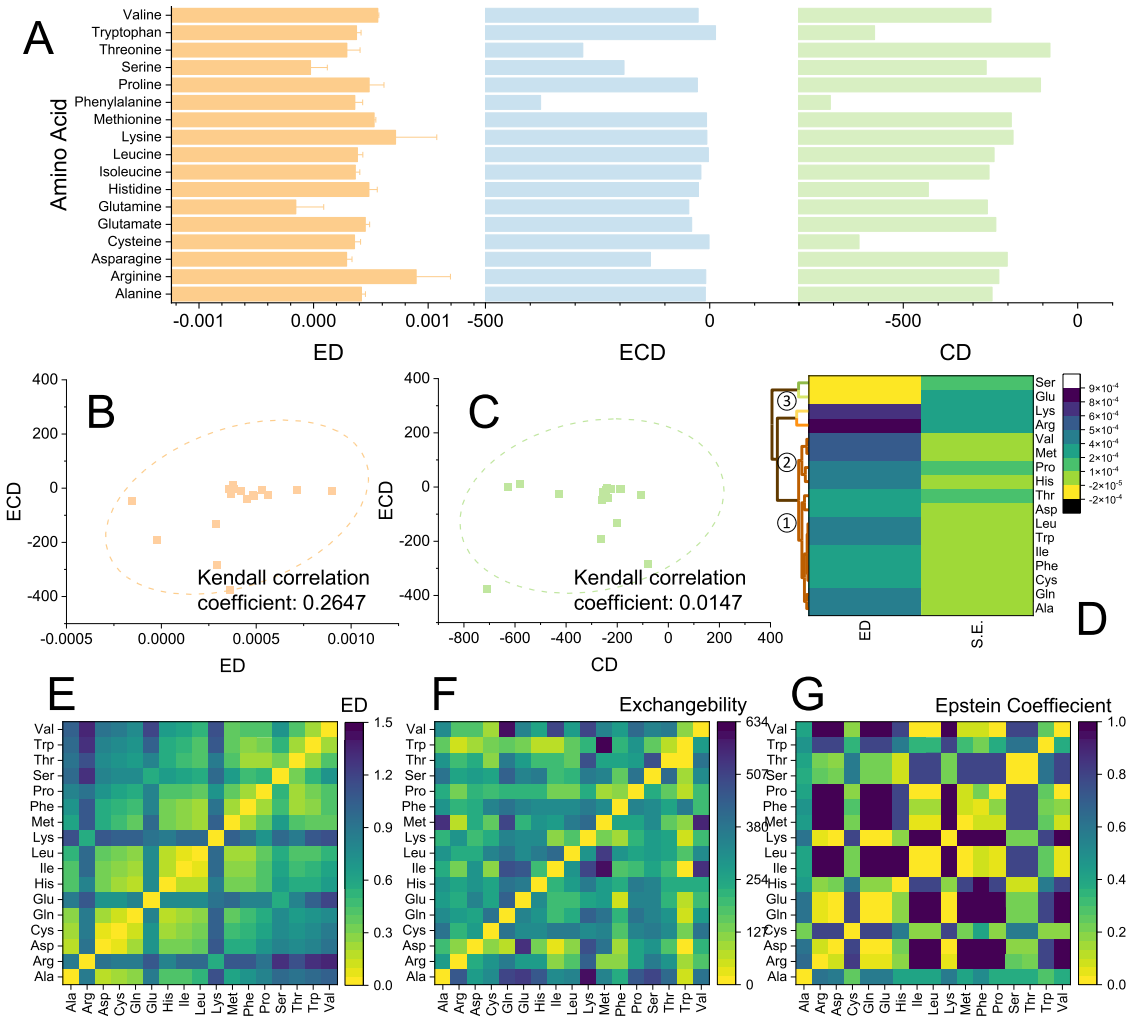

Figure 5. Characterization of amino acids by ED. (**A**) ED and AUC of CD and ECD (electronic circular dichroism) spectra of amino acids. (**B**) and (**C**) Kendall correlation of ECD vs. ED and CD with 95% confidence ellipse. (**D**) ED Cluster Analysis. (**E-G**) Distance map of amino acids based on ED, Exchangeability and Epstein Coeffieicnnet, respectively. Error bars, mean ± s.e.m; n = 4.

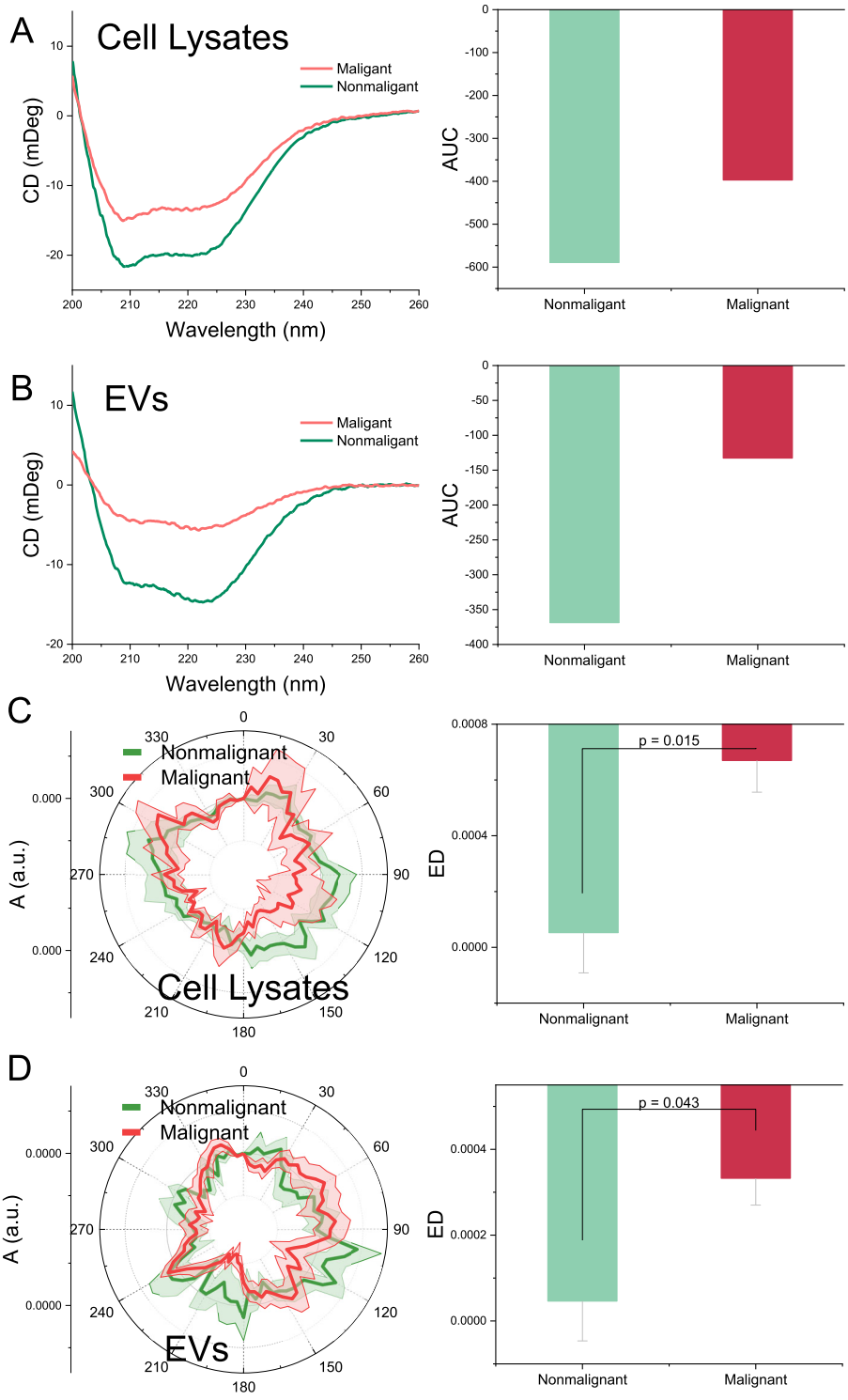

Figure 6. Characterization of b**–sheet-richness of tumorous lysates and EVs by ED.** (**A**) CD spectra and AUC of lysates from malignant and nonmalignant cells. The spectra were averaged from five repeated measurements. (**B**) CD spectra and AUC of EVs from malignant and nonmalignant EVs. (**C**) AS and ED of lysates from malignant and nonmalignant cells. The spectra were averaged from five repeated measurements. (**D**) AS and ED of EVs of malignant and nonmalignant cells. The AS spectra were baseline subtracted. Error bars, mean ± s.e.m; n = 4. Nonmalignant: HPNE; Malignant: MIA PaCa-2. n.s., not significant; p values were determined by unpaired two-tailed t-tests.

Author contributions: DS conceived the idea, provided financial support, supervised the project, conducted the experiments. DS and AB wrote the manuscript. AB, SE and EN assisted with the experiments. DS, WX and IL contributed to editing the manuscript. F , TS and WX contributed to molecular simulation. DS approved the final version of the manuscript.

Competing interests: Authors declare that they have no competing interests.

Data and materials availability: All data are available in the main text or supplementary materials.

Supporting Information

Figure S1. Intensity spectrum of the deuterium lamp used in simulation.

Figure S2. Simple control scheme of ED.

Figure S3. Settling time of the ED spectrometer.

Figure S4. Angle sweeping (AS) results of L amino acids.

Figure S5. CD spectra of amino acids.

Figure S6. Optimized amino acids structures used for TDDFT simulation.

Figure S7. Absorption coefficient (ε) and ECD (Δε) spectra of amino acids.

Figure S8. Molar absorption coefficient of Bovine serum albumin (BSA) used in simulation.

Figure S9. Repeatability and SNR.

Figure S10. Comparison of the baseline models.

Table S1. Waveplate rotation and time stamp.

Table S2. A feature comparison of ED and CD spectrometer.

Movie 1: Polarization ellipse corresponding to θ-scanning

Acknowledgments

The authors acknowledge North Dakota State University Center for Computationally Assisted Science and Technology for computing resources. This work was financially supported by grants from the National Cancer Institute (R03CA252783, R21CA270748) and the National Institute of General Medical Sciences (U54GM128729) of National Institutes of Health to DS, NDSU EPSCoR STEM Research and Education fund (FAR0032086) to DS, ND EPSCoR: Advancing Science Excellence in ND (FAR0030554) to DS, National Science Foundation

(NSF) under NSF EPSCoR Track-1 Cooperative Agreement (OIA #1355466) to DS. NSF under NSF OIA ND-ACES (Award #1946202) to WX, NDSU Foundation and Alumni Association to DS.

References

Ball, D.W., 2006. Field Guide to Spectroscopy, in: Field Guide to Spectroscopy. SPIE Press. https://doi.org/10.1117/3.682726

Becke, A.D., 1998. Density-functional thermochemistry. III. The role of exact exchange. J Chem Phys 98, 5648. https://doi.org/10.1063/1.464913

Bertucci, C., Pistolozzi, M., De Simone, A., 2010. Circular dichroism in drug discovery and development: An abridged review. Anal Bioanal Chem. https://doi.org/10.1007/s00216-010-3959-2

Blakemore, P., 1987. Spectrophotometry and Spectrofluorimetry A Practical Approach. Biochem Educ 15, 159. https://doi.org/10.1016/0307-4412(87)90059-8

Bö, L., Sidler, D., Kittelmann, T., Rgen Stohner, J., Zindel, D., Wagner, T., Riniker, S., 2019. Determination of Absolute Stereochemistry of Flexible Molecules Using a Vibrational Circular Dichroism Spectra Alignment Algorithm. https://doi.org/10.1021/acs.jcim.8b00789

Bulheller, B.M., Hirst, J.D., 2009. DichroCalc—circular and linear dichroism online. Bioinformatics 25, 539–540. https://doi.org/10.1093/BIOINFORMATICS/BTP016

Cerpa, R., Cohen, F.E., Kuntz, I.D., 1996. Conformational switching in designed peptides: the helix/sheet transition. Fold Des 1, 91–101. https://doi.org/10.1016/S1359-0278(96)00018-1

Collett, E., 2005. Optopedia: Wave Plates [WWW Document]. Field Guide to Polarization, SPIE Press, Bellingham, WA.

Comby, A., Bloch, E., Bond, C.M.M., Descamps, D., Miles, J., Petit, S., Rozen, S., Greenwood, J.B., Blanchet, V., Mairesse, Y., 2018. Real-time determination of enantiomeric and isomeric content using photoelectron elliptical dichroism. Nature Communications 2018 9:1 9, 1–14. https://doi.org/10.1038/s41467-018-07609-9

Corrêa, D.H.A., Ramos, C.H.I., 2009. The use of circular dichroism spectroscopy to study protein folding, form and function. African Journal of Biochemistry Research 3, 164–173.

Ding, Y., Li, X.-C., Ferreira, D., 2007. Theoretical Calculation of Electronic Circular Dichroism of the Rotationally Restricted 3,8‘ ‘-Biflavonoid Morelloflavone. J Org Chem 72, 9010–9017. https://doi.org/10.1021/jo071134z

Dinitto, J.M., Kenney, J.M., 2012. Noise characterization in circular dichroism spectroscopy. Appl Spectrosc 66, 180–187. https://doi.org/10.1366/11-06417

Epstein, C.J., 1967. Non-randomness of ammo-acid changes in the evolution of homologous proteins. Nature 215, 355–359. https://doi.org/10.1038/215355a0

Goldstein, D.H., 2017. Polarized light: Third edition, Thrid. ed, Polarized Light. CRC Press. https://doi.org/10.1201/b10436

Greenfield, N.J., 2007a. Using circular dichroism spectra to estimate protein secondary structure. Nature Protocols 2007 1:6 1, 2876–2890. https://doi.org/10.1038/nprot.2006.202

Greenfield, N.J., 2007b. Using circular dichroism spectra to estimate protein secondary structure. Nat Protoc 1, 2876–2890. https://doi.org/10.1038/nprot.2006.202

Greenfield, N.J., 2006. Using circular dichroism spectra to estimate protein secondary structure. Nat Protoc. 1, 2876–2890. https://doi.org/10.1038/nprot.2006.202.Using

He, C., He, H., Chang, J., Chen, B., Ma, H., Booth, M.J., 2021. Polarisation optics for biomedical and clinical applications: a review. Light: Science & Applications 2021 10:1 10, 1–20. https://doi.org/10.1038/s41377-021-00639-x

Kaptein, R., Boelens, R., Scheek, R.M., Van Gunsteren, W.F., 1988. Protein Structures from NMR. Biochemistry 27, 5389–5395. https://doi.org/10.1021/BI00415A001

Kelly, S., Price, N., 2005. The Use of Circular Dichroism in the Investigation of Protein Structure and Function. Curr Protein Pept Sci 1, 349–384. https://doi.org/10.2174/1389203003381315

Kvittingen, L., Sjursnes, B.J., 2020. Demonstrating Basic Properties and Application of Polarimetry Using a Self-Constructed Polarimeter. J Chem Educ 97, 2196–2202. https://doi.org/10.1021/ACS.JCHEMED.9B00763/SUPPL_FILE/ED9B00763_SI_002.DOCX

Lednev, I.K., Karnoup, A.S., Sparrow, M.C., Asher, S.A., 1999. α-Helix Peptide Folding and Unfolding Activation Barriers: A Nanosecond UV Resonance Raman Study. J Am Chem Soc 121, 8074–8086. https://doi.org/10.1021/JA991382F

Li, A., Zhang, T., Zheng, M., Liu, Y., Chen, Z., 2017. Exosomal proteins as potential markers of tumor diagnosis. J Hematol Oncol 10, 1–9. https://doi.org/10.1186/s13045-017-0542-8

Lin, J.F., Wu, J.S., Huang, C.H., Liao, T.T., Chang, C.C., 2011. The application of a rotating-wave-plate stokes polarimeter for measurement of the optical rotation angle. Optik (Stuttg) 122, 14–19. https://doi.org/10.1016/J.IJLEO.2009.10.003

Litvinov, R.I., Faizullin, D.A., Zuev, Y.F., Weisel, J.W., 2012. The α-Helix to β-Sheet Transition in Stretched and Compressed Hydrated Fibrin Clots. Biophys J 103, 1020. https://doi.org/10.1016/J.BPJ.2012.07.046

Martz, E., 2012. Introduction to proteins-structure, function, and motion. Biochemistry and Molecular Biology Education. https://doi.org/10.1002/bmb.20603

Miles, A.J., Wallace, B.A., 2019. Biopharmaceutical applications of protein characterisation by circular dichroism spectroscopy, in: Biophysical Characterization of Proteins in Developing Biopharmaceuticals. pp. 123–152. https://doi.org/10.1016/B978-0-444-64173-1.00006-8

Miles, A.J., Wallace, B.A., 2016. Circular dichroism spectroscopy of membrane proteins. Chem Soc Rev. https://doi.org/10.1039/c5cs00084j

M. J. Frisch, G. W. Trucks, H. B. Schlegel, G.E.S., M. A. Robb, J. R. Cheeseman, G. Scalmani, V. Barone, B.M., G. A. Petersson, H. Nakatsuji, M. Caricato, X. Li, H.P.H., A. F. Izmaylov, J. Bloino, G. Zheng, J. L. Sonnenberg, M.H., M. Ehara, K. Toyota, R. Fukuda, J. Hasegawa, M. Ishida, T.N., Y. Honda, O. Kitao, H. Nakai, T. Vreven, J. A. Montgomery, Jr., J. E. Peralta, F. Ogliaro, M. Bearpark, J. J. Heyd, E.B., K. N. Kudin, V. N. Staroverov, T. Keith, R. Kobayashi, J.N., K. Raghavachari, A. Rendell, J. C. Burant, S. S. Iyengar, J.T., M. Cossi, N. Rega, J. M. Millam, M. Klene, J. E. Knox, J.B.C., V. Bakken, C. Adamo, J. Jaramillo, R. Gomperts, R.E.S., O. Yazyev, A. J. Austin, R. Cammi, C. Pomelli, J.W.O., R. L. Martin, K. Morokuma, V. G. Zakrzewski, G.A.V., P. Salvador, J. J. Dannenberg, S. Dapprich, A.D.D., O. Farkas, J. B. Foresman, J. V. Ortiz, J.C., and D. J. Fox, n.d. Gaussian 09, Revision B.01,. Gaussian, Inc., Wallingford CT,.

Morillas, M., Vanik, D.L., Surewicz, W.K., 2001. On the mechanism of α-helix to β-sheet transition in the recombinant prion protein. Biochemistry 40, 6982–6987. https://doi.org/10.1021/bi010232q

Pedrotti, F.L., Pedrotti, L.M., Pedrotti, L.S., 2017. Introduction to Optics, Introduction to Optics. Cambridge University Press. https://doi.org/10.1017/9781108552493

Pelton, J.T., McLean, L.R., 2000. Spectroscopic methods for analysis of protein secondary structure. Anal Biochem 277, 167–176. https://doi.org/10.1006/abio.1999.4320

Petersson, G.A., Bennett, A., Tensfeldt, T.G., Al-Laham, M.A., Shirley, W.A., Mantzaris, J., 1998. A complete basis set model chemistry. I. The total energies of closed-shell atoms and hydrides of the first-row elements. J Chem Phys 89, 2193. https://doi.org/10.1063/1.455064

Pham, T.-T.-H., Lo, Y.-L., 2012. Extraction of effective parameters of turbid media utilizing the Mueller matrix approach: study of glucose sensing. J Biomed Opt 17, 0970021. https://doi.org/10.1117/1.jbo.17.9.097002
Phan, Q.H., Han, C.Y., Lien, C.H., Pham, T.T.H., 2021. Dual-Retarder Mueller Polarimetry System for Extraction of Optical Properties of Serum Albumin Protein Media. Sensors (Basel) 21. https://doi.org/10.3390/S21103442
Rasuleva, K., Elamurugan, S., Bauer, A., Khan, M., Wen, Q., Li, Z., Steen, P., Guo, A., Xia, W., Mathew, S., Jansen, R., Sun, D., 2021a. β-Sheet Richness of the Circulating Tumor-Derived Extracellular Vesicles for Noninvasive Pancreatic Cancer Screening. ACS Sens 6, 4489–4498. https://doi.org/10.1021/acssensors.1c02022
Rasuleva, K., Elamurugan, S., Bauer, A., Khan, M., Wen, Q., Li, Z., Steen, P., Guo, A., Xia, W., Mathew, S., Jansen, R., Sun, D., 2021b. β-Sheet Richness of the Circulating Tumor-Derived Extracellular Vesicles for Noninvasive Pancreatic Cancer Screening. ACS Sens. https://doi.org/10.1021/ACSSENSORS.1C02022/SUPPL_FILE/SE1C02022_SI_001.PDF
Šali, A., 1998. 100,000 protein structures for the biologist, in: Nature Structural Biology. Nature Publishing Group, pp. 1029–1032. https://doi.org/10.1038/4136
Schellman, J.A., 1975. Circular Dichroism and Optical Rotation. Chem Rev 75, 323–331. https://doi.org/10.1021/cr60295a004
Sreerama, N., Woody, R.W., 2000. Estimation of protein secondary structure from circular dichroism spectra: comparison of CONTIN, SELCON, and CDSSTR methods with an expanded reference set. Anal Biochem 287, 252–260. https://doi.org/10.1006/ABIO.2000.4880
Stephens, P.J., Harada, N., 2010. ECD cotton effect approximated by the Gaussian curve and other methods. Chirality 22, 229–233. https://doi.org/10.1002/CHIR.20733
Sun, D., Zhao, Z., Spiegel, S., Liu, Y., Fan, J., Amrollahi, P., Hu, J., Lyon, C.J., Wan, M., Hu, T.Y., 2021. Dye-free spectrophotometric measurement of nucleic acid-to-protein ratio for cell-selective extracellular vesicle discrimination. Biosens Bioelectron 179, 113058. https://doi.org/10.1016/j.bios.2021.113058
Swinehart, D.F., 1962. The Beer-Lambert law. J Chem Educ 39, 333–335. https://doi.org/10.1021/ED039P333
Teare, S.W., 2017. Optics Using MATLAB, Optics Using MATLAB. SPIE. https://doi.org/10.1117/3.2266670
Venyaminov, S.Y., Vassilenko, K.S., 1994. Determination of protein tertiary structure class from circular dichroism spectra. Anal Biochem 222, 176–184. https://doi.org/10.1006/abio.1994.1470
Vogel, M., 2022. Mueller-Stokes-Jones Calculus [WWW Document]. MATLAB Central File Exchange. URL https://www.mathworks.com/matlabcentral/fileexchange/45087-mueller-stokes-jones-calculus (accessed 2.6.22).
Warnke, I., Furche, F., 2012. Circular dichroism: Electronic. Wiley Interdiscip Rev Comput Mol Sci 2, 150–166. https://doi.org/10.1002/wcms.55
Whitmore, L., Wallace, B.A., 2004. DICHROWEB, an online server for protein secondary structure analyses from circular dichroism spectroscopic data. Nucleic Acids Res 32, W668. https://doi.org/10.1093/NAR/GKH371
Yampolsky, L.Y., Stoltzfus, A., 2005. The exchangeability of amino acids in proteins. Genetics 170, 1459–1472. https://doi.org/10.1534/genetics.104.039107
Yang, Z., Albrow-Owen, T., Cai, W., Hasan, T., 2021a. Miniaturization of optical spectrometers. Science (1979) 371. https://doi.org/10.1126/science.abe0722
Yang, Z., Albrow-Owen, T., Cai, W., Hasan, T., 2021b. Miniaturization of optical spectrometers. Science (1979) 371. https://doi.org/10.1126/science.abe0722

TOC

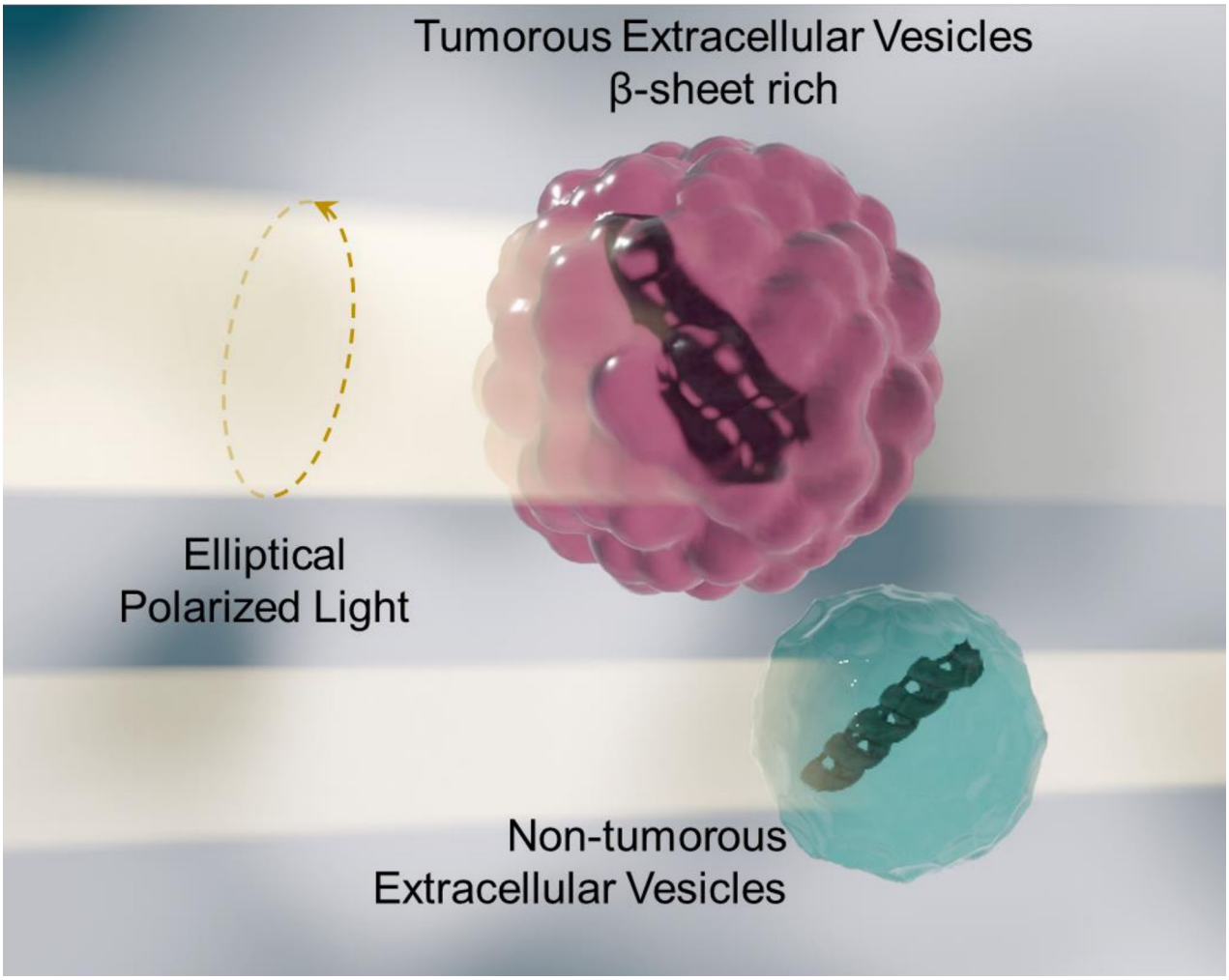

B-sheet rich tumorous extracellular vesicles absorb more left elliptical polarized light than the nontumorous counterparts, which can be sensed by elliptical dichroism.

Supplementary Information for

A Portable Elliptical Dichroism Spectrometer Targeting Secondary Structural Features of Tumorous Protein for Pancreatic Cancer Detection

Aaron Bauer, Santhalingam Elamurugan, Sara Tolba Selim, Fatima, Ejjigu Nega, Ivan T. Lima Jr., Wenjie Xia, Dali Sun*

*Dali Sun. Email: dali.sun@ndsu.edu.

This PDF file includes:

Figures S1 to S10
Tables S1 to S2
SI References

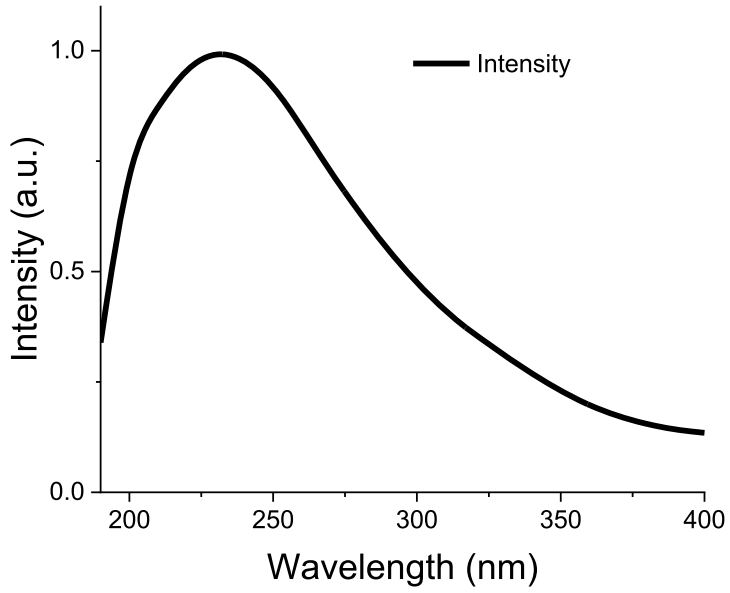

Fig. S1. Intensity spectrum of the deuterium lamp used in simulation.

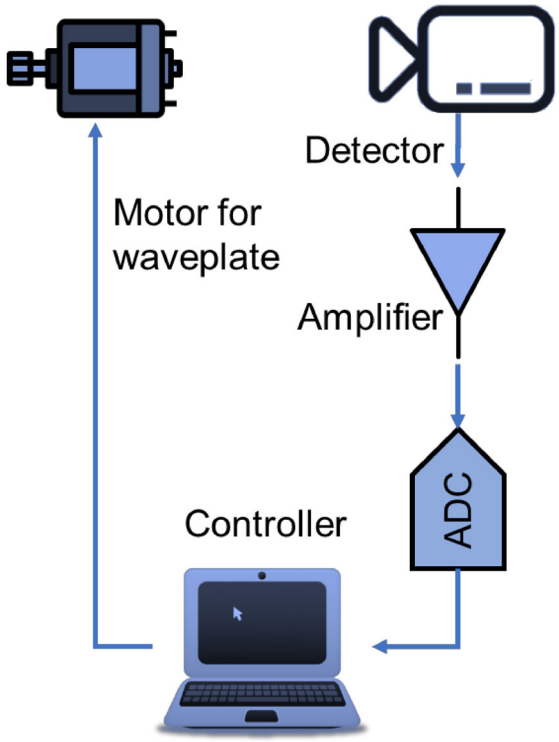

Fig. S2. Simple control scheme of ED.

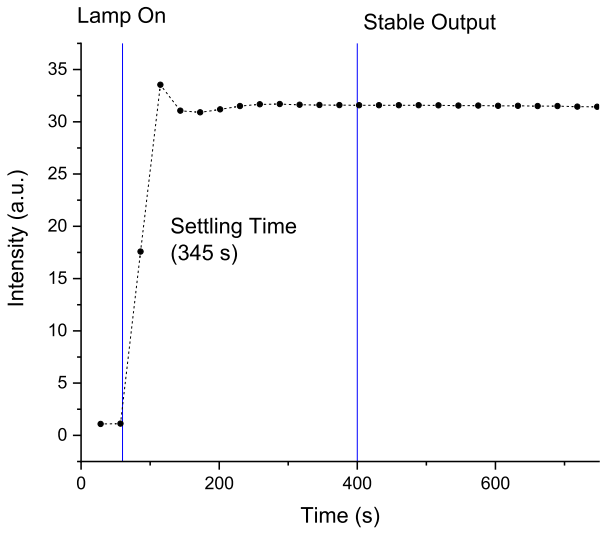

Fig. S3. Settling time of the elliptical dichroism (ED) spectrometer.

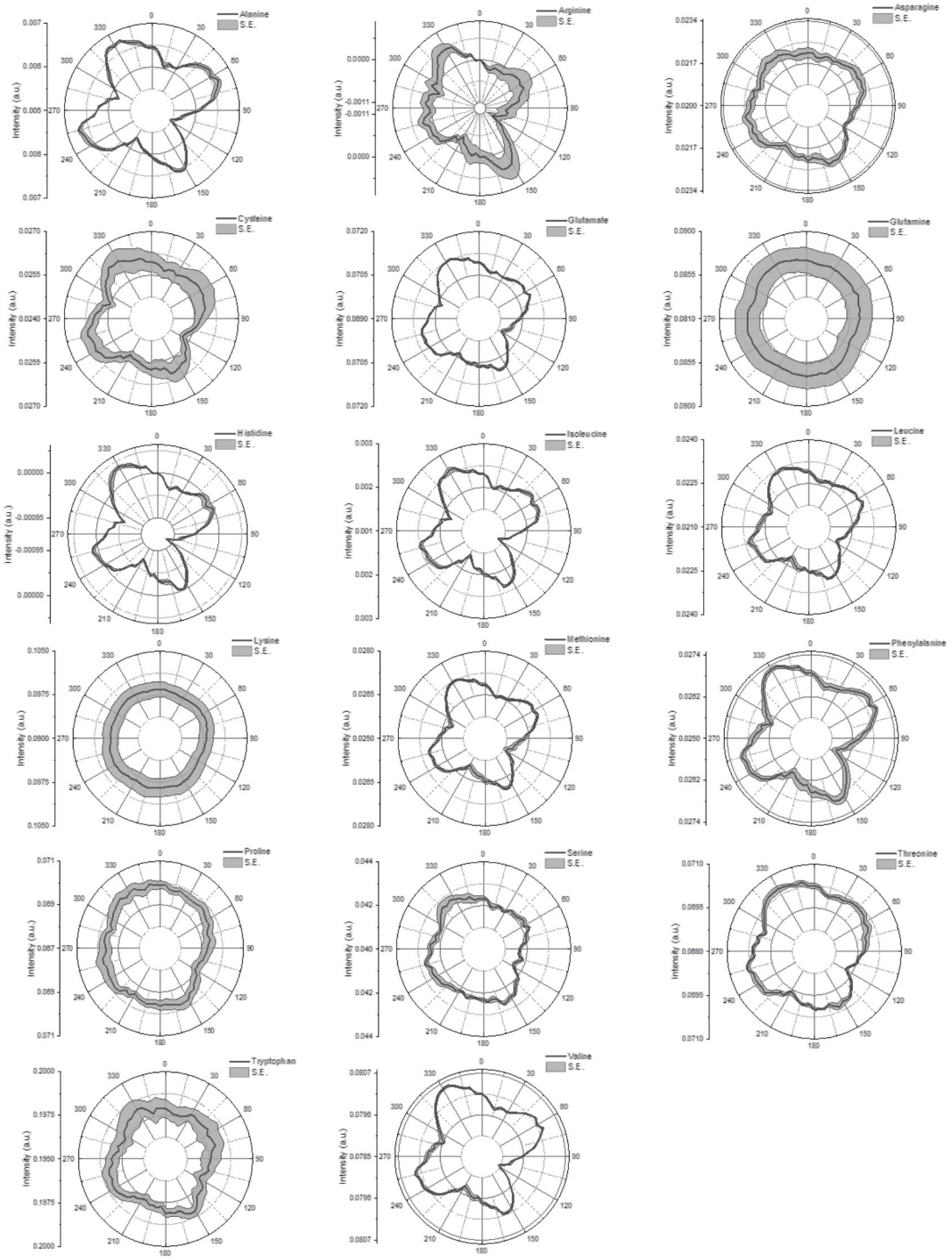

Fig. S4. Angle sweeping (AS) results of L amino acids.

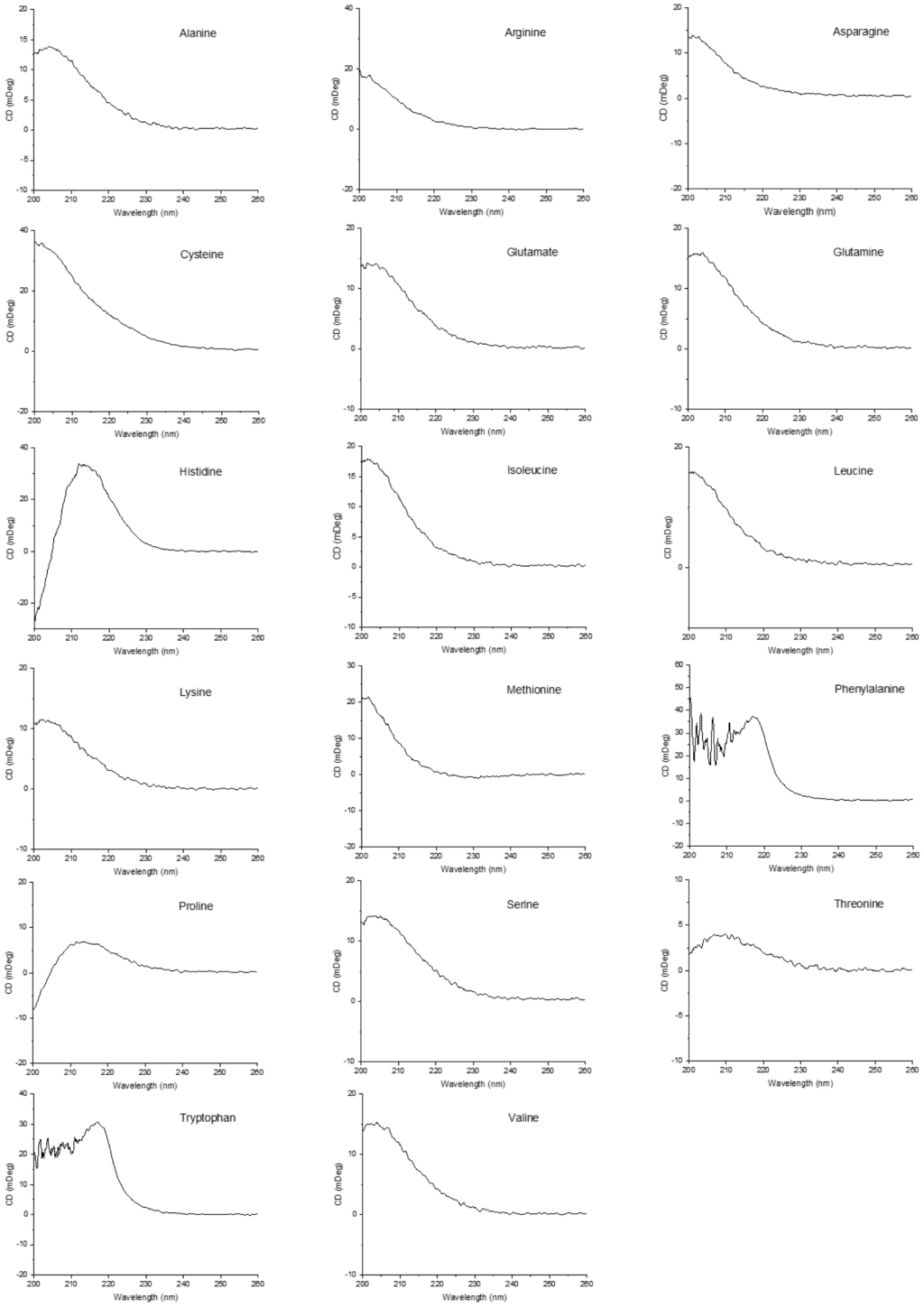

Fig. S5. Circular dichroism (CD) spectra of L amino acids.

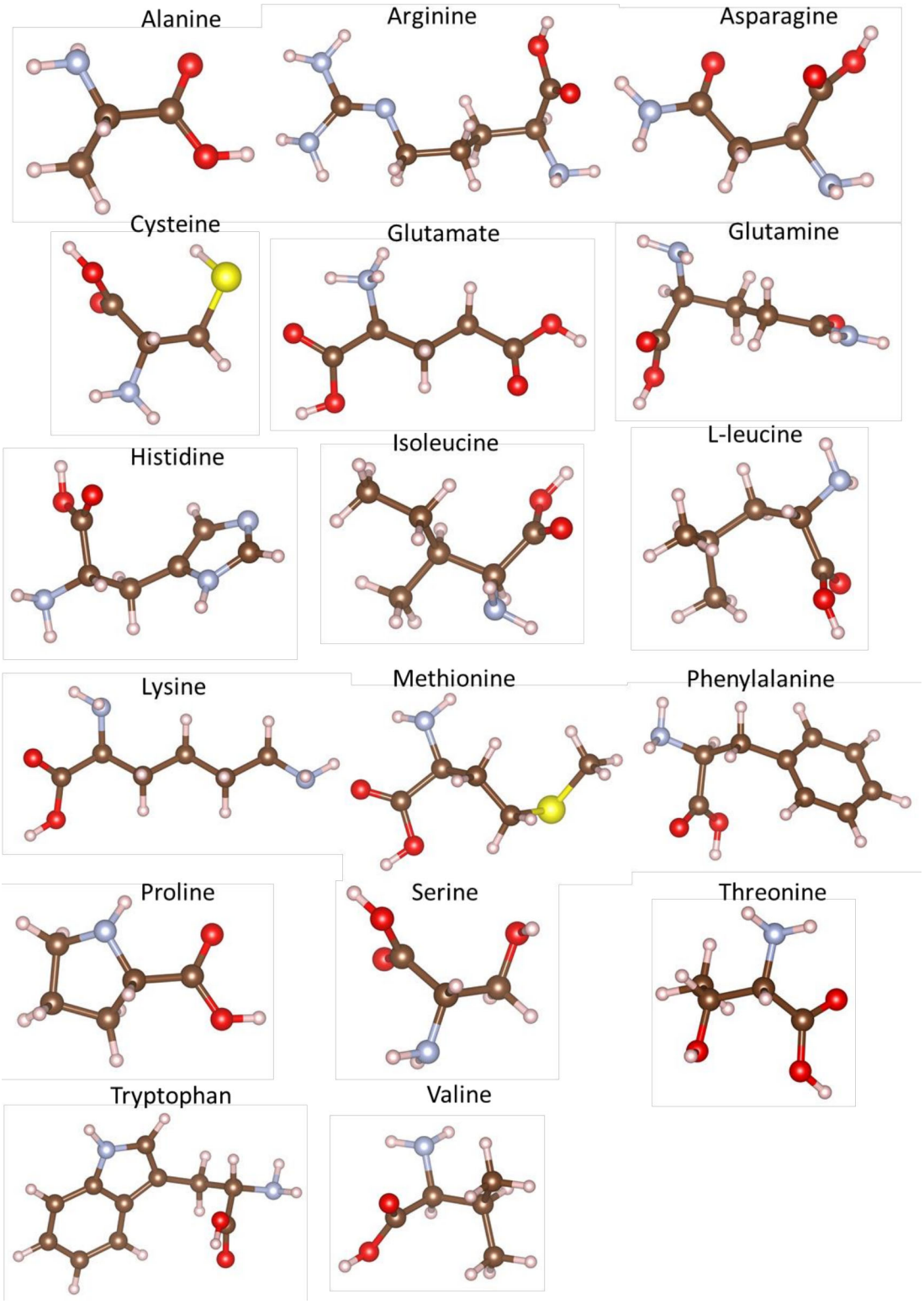

Fig. S6. Optimized amino acids structures used for time-dependent density-functional theory (TDDFT) simulation.

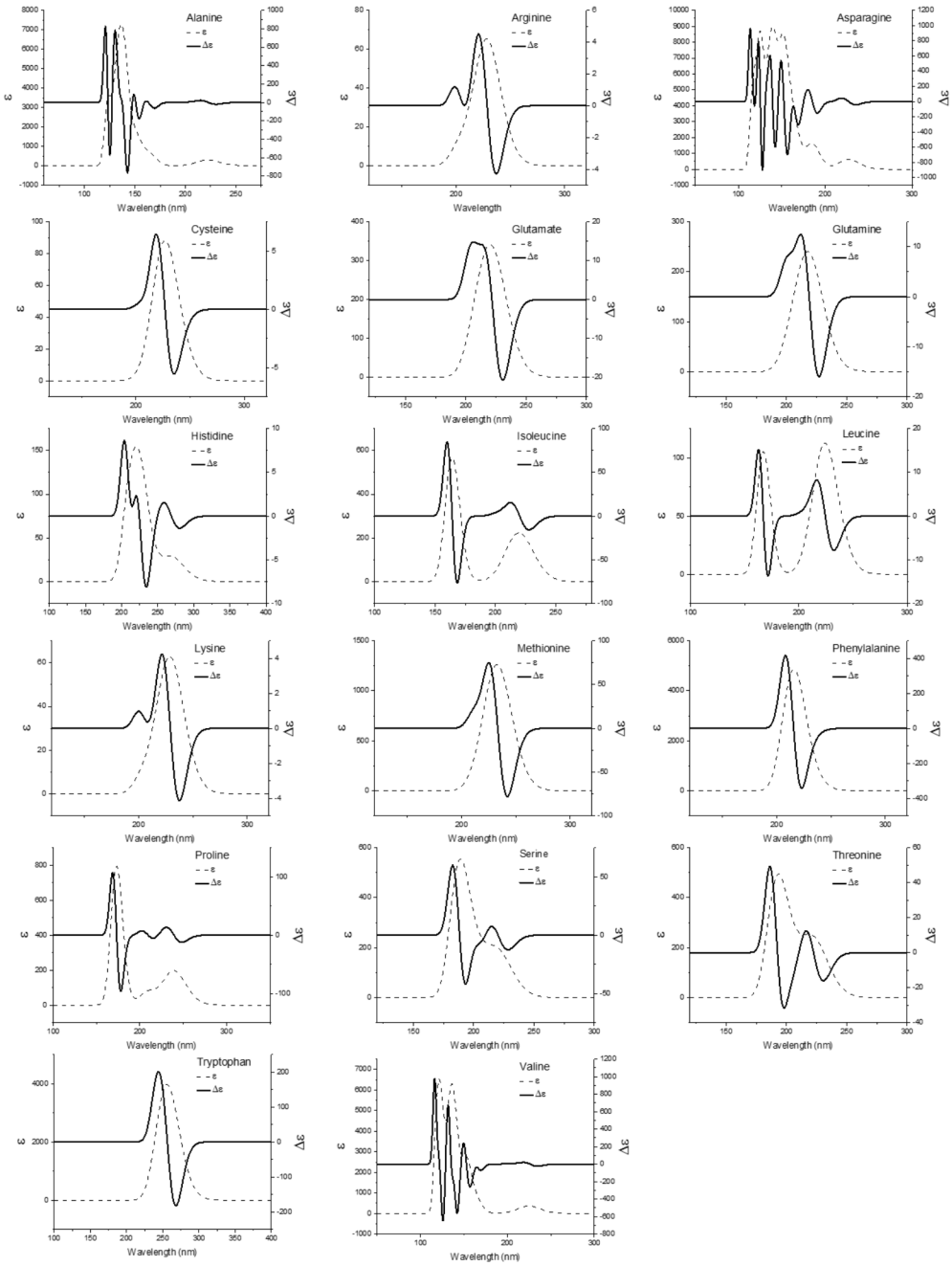

Fig. S7. Absorption coefficient (ε) and electronic circular dichroism (ECD) (Δε) spectra of L amino acids.

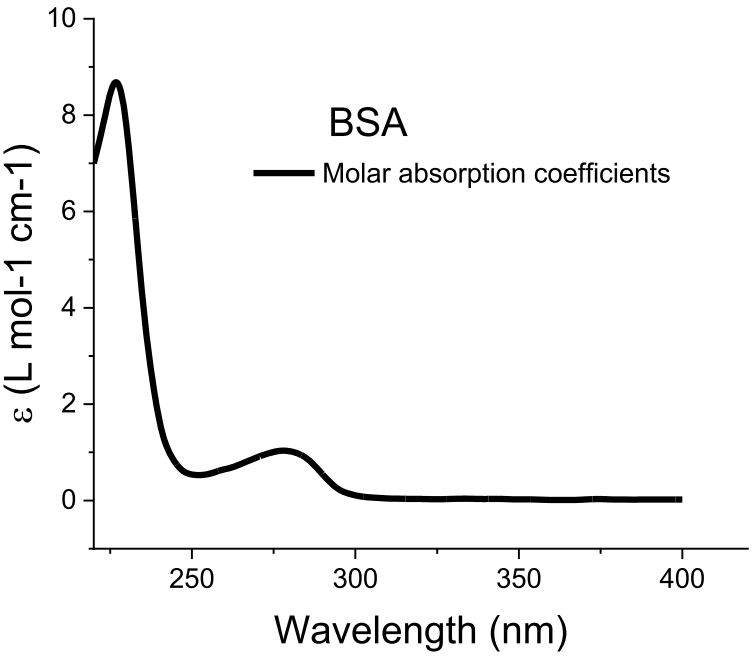

Fig. S8. Molar absorption coefficient of Bovine serum albumin (BSA) used in simulation, measured by NanoDrop (Thermo Scientific).

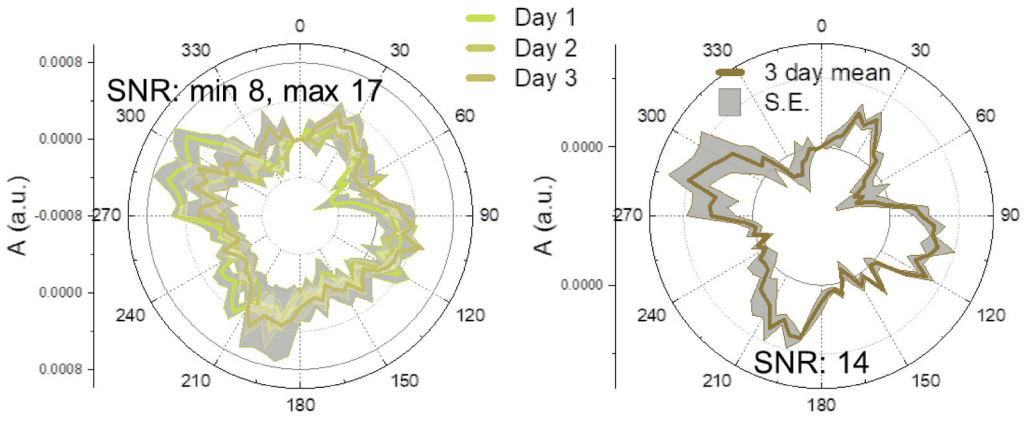

Fig. S9. Repeatability and signal-to-noise ratio (SNR). SNR is defined as mean/standard deviation(*1*)**.**

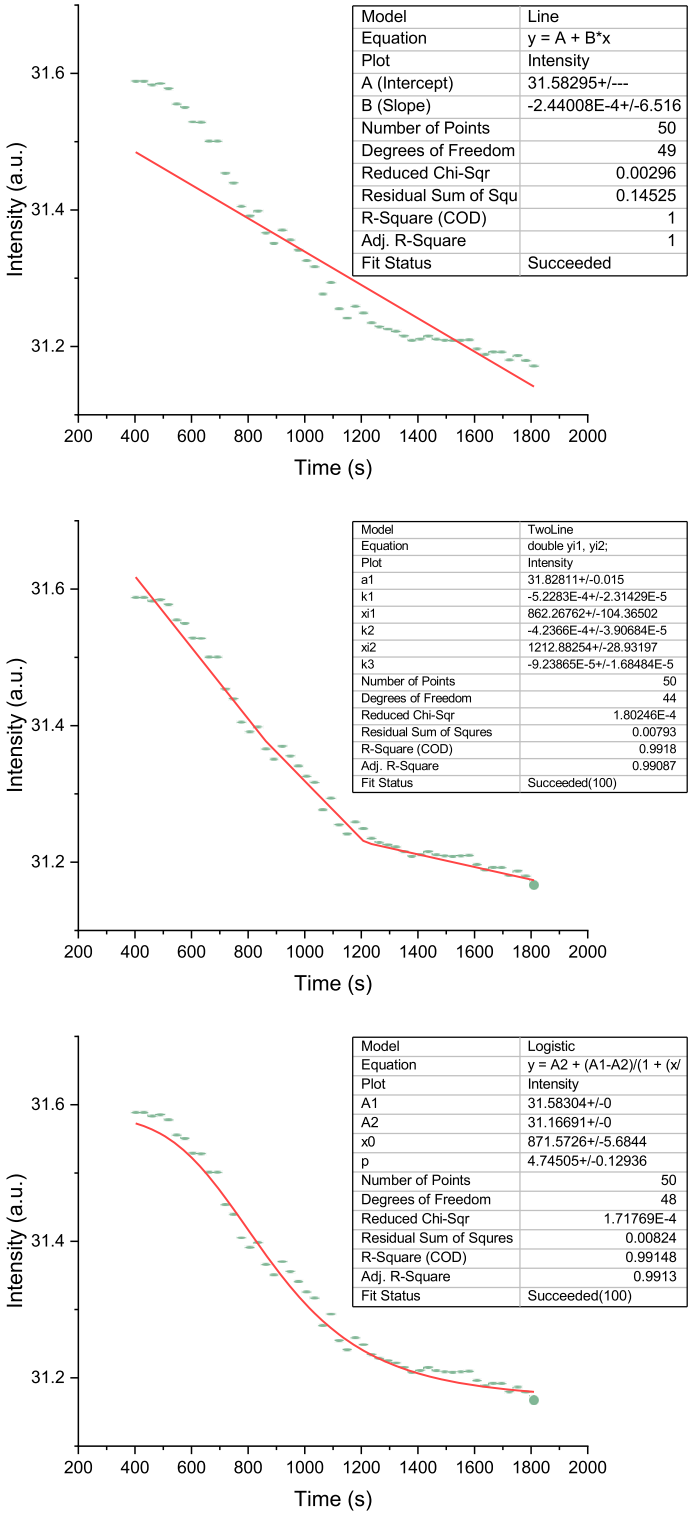

Fig. S10. Comparison of the baseline models.

Table S1. Waveplate rotation and time stamp.

Theta(°)	Time(S)	Theta(°)	Time(S)	Theta(°)	Time(S)	Theta(°)	Time(S)
0	12	90	246	180	479	270	714
5	25	95	259	185	492	275	727
10	38	100	272	190	506	280	740
15	51	105	285	195	519	285	753
20	64	110	298	200	532	290	766
25	77	115	311	205	545	295	779
30	90	120	324	210	558	300	792
35	103	125	337	215	571	305	805
40	116	130	349	220	584	310	818
45	129	135	362	225	597	315	831
50	142	140	375	230	610	320	844
55	155	145	388	235	623	325	857
60	168	150	401	240	636	330	870
65	181	155	414	245	649	335	883
70	194	160	427	250	662	340	896
75	207	165	441	255	675	345	909
80	220	170	454	260	688	350	922
85	233	175	467	265	701	355	935

Table S2. A feature comparison of ED and CD spectrometer

FEATURE	CD	ED
LIMIT OF DETECTION (mg/mL*)	**0.25**	**0.5**
SIGNAL-TO-NOISE RATIO	**20**	**14**
REPEATABILITY (CV,%)	**0.5**	**18**
INTERVAL OF DETECTION (min)	**1**	**15**
STABILITY (3 DAYS, %)	**95**	**78**

* For protein structural analysis only. All experiment was conducted using the same protein (Chymotrypsin) under the same condition.

SI References

1. J. Hanlan, D. A. Skoog, D. M. West, (1973), p. 47.